Image-Based Method for Dual Energy Computed Tomography Image Decomposition

Nurul Afiqah Ramlan [a], Hang See Pheng [b]*

[a,b]Department of Mathematical Sciences, Faculty of Science, Universiti Teknologi Malaysia,
81310 Johor Bahru, Johor, Malaysia.
*Corresponding author: sphang@utm.my

Abstract

This study focuses on implementing image-based method to perform material decomposition on ex-vivo samples and microchips through Dual Energy Computed Tomography (DECT) images. The image-based method is computer-based system that consist of mathematical equations that can differentiate DECT images and obtain the material-specific image of object. From the results, it is found that the appropriate linear attenuation coefficients (HU) can provide good visualization in the material-specified images. The input DECT image produced at angle 270° provide comprehensive view of each core material of microchip through the material-specified images. The image-based method is useful for microCT imaging laboratories and assessing quality of microchips in industry.

Keywords: Image-based method, Dual energy computed tomography (DECT), Material decomposition

1   Introduction

Dual energy computed tomography (DECT) is a medical imaging method which is able to produce images based on two data sets from the same anatomic location with different energy (kVp). DECT was conceived at the very beginning of the computed tomography era and the first DECT scanner was developed in 2006 [1]. For more than a decade, microCT using ex-vivo samples have been used for bone phenotyping, as bone has sufficient intrinsic x-ray absorption for high contrast x-ray imaging [2]. In industry, material decomposition using DECT has been used in the field counterfeit gold, rock characterization, determine moisture content inside the wood, material differentiation in forensic radiology, and baggage security screening [3][4]. Some clinically relevant imaging applications with high diagnostic accuracy and differentiate material for industry have been developed and reported. For example, it can differentiate the metal artefacts from a double hip-joint-prosthesis, can detect gout by differentiating between uric acid and calcium by their material-specific dual energy properties, differentiate tumours, subtypes pathologic grades, and molecular subcategories of lung cancers, distinguishing calcific from haemorrhagic cerebral, and use for detection of micro calcifications in breast imaging [5].

In this research, two experiments are conducted for ex-vivo samples that were publicly available from article published by Handschuh [6] and primary dataset of microchip CT images is collected from Malaysian Nuclear Agency, Kajang. The ex-vivo is the image samples that have been extracted from the organism, not created artificially but directly taken from a living

organism through images. In this study, sample image for juvenile sturgeon is used. Furthermore, a microchip with no defect is important to make sure the machine is well-functioning. Therefore, the image-based method will be implemented in differentiating the component of the microchip's material-specific. This study is expected to be helpful in medical and biology laboratory field and assisting the engineer and inspector in semi-conductor industry to investigate the quality of the microchips automatically.

2 Problem Statement

The manual inspection on the numerous of images to investigate the ex-vivo samples and structure of quality of products is challenging in industry. This is due to the manual inspection is an obscure and very time-consuming task moreover if the sample is in micro size. Standard microchips are typically 11–13 mm long and 2 mm in diameter which is small enough to do inspection by eyes. A computer-based system with the help of mathematical approaches and proper parameters in image processing are crucial to differentiate the image and obtain the material-specific image.

3 Methodology of Image Decomposition

The methodology of image decomposition on DECT image is described in the following sub-section. For material decomposition, both the numerically simulated and experimentally acquired images are performed in the experimental stage to ensure the material-specification can be done effectively on the DECT images. The grey-scale values within each material-specific image represented the percentage of material present within a voxel will be also revealed in this paper.

3.1 Image-based Method

The image-based method implemented on the dual energy computed tomography (DECT) images generated by two different energies. The reconstructed registered image in TIFF is used, these images are then converted to 16-bit unsigned format, and finally, the image-based method is implemented using MATLAB software. Image-based method typically reconstructs each polychromatic raw data set separately using common image reconstruction methods such as filtered back-projection (FBP), and then perform linear combinations of the images from every spectrum to obtain the two basis material images. With a polychromatic X-Ray spectrum, X-ray attenuation is given by the Equation 1 below, with the spatial integration along with a path L

$$A = \frac{I}{I_0} = \frac{\int_{\hat{E}} S(E)D(E)e^{-\int_L \mu(E,\vec{r})d\vec{r}}dE}{\int_{\hat{E}} S(E)D(E)dE} \tag{1}$$

where I and I_0 are the X-ray attenuated and initial intensities, respectively, $\hat{E}$ denotes the energy range of detected X-rays, $S(E)$ and $D(E)$ represents the x-ray spectrum and detector response function at energy E, respectively, and $\mu(E,\vec{r})$ is the spectral attenuation coefficient of the material at position $\vec{r}$.
A system weighting function was defined as,

$$w_{\hat{E}}(E) = \frac{S(E)D(E)}{\int_{\hat{E}} S(E\prime)D(E\prime)dE\prime} \tag{2}$$

Different system weighting functions reflect different polychromatic computed tomography (CT) measurements. Substitute Equation (2) into Equation (1),

$$A = \int_{\hat{E}} w_{\hat{E}}(E) e^{-\int_L \mu(E,\vec{r})d\vec{r}} dE \tag{3}$$

For a monoenergetic X-ray source, $E = E_0$, $w_{\hat{E}}(E) = \delta(E - E_0)$, Equation (3) is simplified to

$$In(A) = -\int_L \mu(E_0, \vec{r})\, d\vec{r}, \tag{4}$$

which was equivalent to a Radon transform. For a polychromatic CT, the spectral attenuation coefficients $\mu(E, \vec{r})$ are described by a linear combination of basis functions

$$\mu(E, \vec{r}) = c_1(\vec{r})f_1(E) + c_2(\vec{r})f_2(E) + \cdots + c_N(\vec{r})f_N(E) \tag{5}$$

where $c_1, c_2, \ldots, c_N$ are the spatially dependent concentration of N different basis materials and $f_1 + f_2 + \cdots + f_N$ the energy dependent basis functions, or the linear attenuation coefficients of the basis materials alone at energy E. This superposition separated energy E and position $\vec{r}$. The effective linear attenuation coefficient $\bar{\mu}_I(\vec{r})$ at energy $\hat{E}_i$ was computed as

$$\bar{\mu}_I(\vec{r}) = \int_{\hat{E}} w_{\hat{E}}(E)\mu(E,\vec{r})dE \tag{6}$$
$$= \int_{\hat{E}} w_{\hat{E}}(E) \sum_{j=1}^{N} c_j(\vec{r})\, f_j(E)dE \tag{7}$$
$$= \sum_{j=1}^{N} c_j(\vec{r}) \int_{\hat{E}} w_{\hat{E}}(E)f_j(E)dE \tag{8}$$
$$= \sum_{j=1}^{N} c_j(\vec{r})\, K_{i,j} \tag{9}$$

where

$$K_{i,j} = \int_{\hat{E}} w_{\hat{E}}(E)f_j(E)dE \tag{10}$$

representing the effective linear attenuation coefficient of basis material j within the energy bin $\hat{E}$. Equation (9) then can be expressed in a matrix notation

$$\begin{bmatrix} \bar{\mu}_1(\vec{r}) \\ \bar{\mu}_2(\vec{r}) \\ \cdots \\ \bar{\mu}_i(\vec{r}) \\ \cdots \\ \bar{\mu}_n(\vec{r}) \end{bmatrix} = \begin{bmatrix} K_{1,1} & \cdots & K_{1,N} \\ \vdots & \ddots & \vdots \\ K_{n,1} & \cdots & K_{n,N} \end{bmatrix} \begin{bmatrix} c_1(\vec{r}) \\ c_2(\vec{r}) \\ \cdots \\ c_i(\vec{r}) \\ \cdots \\ c_N(\vec{r}) \end{bmatrix} \tag{11}$$

with element $\bar{\mu}_i(\vec{r})$ representing the effective linear attenuation coefficient of the unknown material at energy $\hat{E}$ and position $\vec{r}$ while element $c_i(\vec{r})$ denoted the concentration information of basis material i at position $\vec{r}$ in the unknown object.

3.2 Decomposition of material
To decompose material in the images, the Hounsfield Units (HU) are used. The HU value make up by the grayscale in medical CT imaging, it is a scale from black to white of 4096 values (12 bit) and ranges from -1024 HU to 3071 HU [9] in each voxel of the CT images. The ability of computed tomography to quantify X-ray attenuation in HU value is beneficial for the identification of objects. The HU value are also known as effective linear attenuation coefficient μ. In section 3.1,

the effective linear attenuation coefficient μ measured in each volume element (voxel) of a CT image, can be expressed as a linear combination of the attenuation coefficients of the basis materials multiplied by their volume fraction,

$$F_{material\ 1} \cdot \mu_{material\ 1,E} + F_{material\ 2} \cdot \mu_{material\ 2,E} + F_{material\ 3} \cdot \mu_{material\ 3,E} = \mu_E \quad (12)$$

In Equation (12), $\mu_{material\ 1,E}$, $\mu_{material\ 2,E}$, and $\mu_{material\ 3,E}$ are the effective linear attenuation coefficients acquired in regions of interests with 100% content of material 1, material 2, and material 3 at the two energies, respectively, and $F_{material\ 1}$, $F_{material\ 2}$, and $F_{material\ 3}$ represent the volume fractions of the three basis materials. If a voxel contains only three basis materials, the sum of the volume fractions must add to unity,

$$F_{material\ 1} + F_{material\ 2} + F_{material\ 3} = 1 \quad (13)$$

to use dual-energy method, two CT images are acquired with mean energies *E1* and *E2*, two independent measurements are made of the attenuation coefficients as follows,

$$F_{material\ 1} \cdot \mu_{material\ 1,E1} + F_{material\ 2} \cdot \mu_{material\ 2,E1} + F_{material\ 3} \cdot \mu_{material\ 3,E1} = \mu_{E1} \quad (14)$$

$$F_{material\ 1} \cdot \mu_{material\ 1,E2} + F_{material\ 2} \cdot \mu_{material\ 2,E2} + F_{material\ 3} \cdot \mu_{material\ 3,E2} = \mu_{E2} \quad (15)$$

The linear attenuation coefficients for the basis materials $F_{material\ 1}$, $F_{material\ 2}$, and $F_{material\ 3}$ at each energy can be measured from the CT images within regions known to contain the respective basis materials.

The unknowns materials $F_{material\ 1}$, $F_{material\ 2}$, and $F_{material\ 3}$ can be found using matrix factorization,

$$AB = X$$
$$B = A^{-1}X$$

$$\begin{bmatrix} F_{material\ 1} \cdot \mu_{material\ 1,E1} + F_{material\ 2} \cdot \mu_{material\ 2,E1} + F_{material\ 3} \cdot \mu_{material\ 3,E1} \\ F_{material\ 1} \cdot \mu_{material\ 1,E1} + F_{material\ 2} \cdot \mu_{material\ 2,E1} + F_{material\ 3} \cdot \mu_{material\ 3,E1} \\ F_{material\ 1} + F_{material\ 2} + F_{material\ 3} \end{bmatrix} = \begin{bmatrix} \mu_{E1} \\ \mu_{E2} \\ 1 \end{bmatrix} \quad (16)$$

$$\begin{bmatrix} \mu_{F_{material\ 1},E1} & \mu_{material\ 2,E1} & \mu_{material\ 3,E1} \\ \mu_{F_{material\ 1},E2} & \mu_{material\ 2,E2} & \mu_{material\ 3,E2} \\ 1 & 1 & 1 \end{bmatrix} \begin{bmatrix} F_{material\ 1} \\ F_{material\ 2} \\ F_{material\ 3} \end{bmatrix} = \begin{bmatrix} \mu_{E1} \\ \mu_{E2} \\ 1 \end{bmatrix} \quad (17)$$

Followed by,

$$\begin{bmatrix} F_{material\ 1} \\ F_{material\ 2} \\ F_{material\ 3} \end{bmatrix} = \begin{bmatrix} \mu_{material\ 1,E1} & \mu_{material\ 2,E1} & \mu_{material\ 3,E1} \\ \mu_{material\ 1,E2} & \mu_{material\ 2,E2} & \mu_{material\ 3,E2} \\ 1 & 1 & 1 \end{bmatrix}^{-1} \begin{bmatrix} \mu_{E1} \\ \mu_{E2} \\ 1 \end{bmatrix} \quad (18)$$

The dual- energy decomposition algorithms will be solved using MATLAB and compiled for material decomposition of both the numerically simulated and experimentally acquired images.

The study implemented the image-based methods to process each volume element (voxel) of a CT image based on the linear combination of the attenuation coefficients of the basis

materials multiplied by their volume fraction. It is concluded that the image-based algorithm is simple and can be directly applied on any microCT setups without any hardware modifications.

4   Results

In the first experiment, the image-based method is implemented by using ex-vivo samples that are available in the research article [6]. The aim of experiment is to analyse the linear attenuation coefficients for different materials or tissues on DECT images. Further, the second experiment employ the primary dataset that collected from Malaysian Nuclear Agency, Kajang to solve the image decomposition problem for microchips sample.

4.1   Image decomposition for ex-vivo sample

A publicly available dataset is used in the first experiment to perform image decomposition. This dataset consists of ex-vivo samples which is juvenile sturgeon for the decomposition of mineralized tissue and soft tissue. The contrast agents are used for staining of tissue sections, with this after have done image-based method we can see more clearly the tissue stained by contrast agent. Figure 1 shows the image of juvenile sturgeon at side position. The dual energy computed tomography (DECT) images used in this experiment are the cross-sectional images of head juvenile (labeled by dotted red line) at two different energy levels which are 40 kVp and 80 kVp. The expected result of image-based method will differentiate the tissues and organs in material-specified images.

The juvenile sturgeon sample were obtained in 2001 from the Conte Anadromous Fish Research Center, Turners Falls, MA, USA. It was fixed in Dent's fixative (80:20 methanol:dimethylsulfoxide) and stored in absolute methanol. It was stained with 1% (w/v) PMA in 100% methanol for 20 h. After staining, it was washed in absolute methanol for several hours and mounted in 0.5% low melt agarose in a 5000 µL micropipette tip. The constrast agent (HA and I2KI) were absorbed inside the sample.
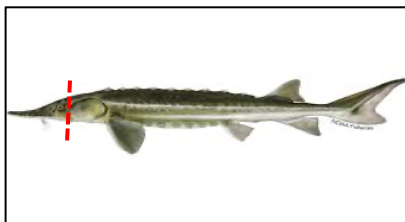

Figure 1: Juvenile sturgeon images

Table 1: Effective linear attenuation coefficients of material are obtained from calibration phantoms

Energy (kVp)	HA	I2KI	Water
40	22253.9	18507.0	0
80	10869.2	23222.1	0

Table 1 shows data effective linear attenuation coefficients of material are obtained from calibration phantoms has been provided by Badea, Piantadosi and Clark [7]. It should be roughly comparable to material concentrations present in the actual samples. Figure 2 are the results of material decomposition by image-based method. There are 3 materials that have been

extracted from the dual energy CT images, the contrast agent HA, PMA, and water. Material 1 image is bone (HA) image of the sturgeon after material decomposition. Material 2 is soft tissue (PMA) image of the sturgeon head after material decomposition in Material 3 which is water images are also the result of three-material-decomposition based on dual-energy scanning and offer a high-contrast 'brightfield' image of the sample that might be useful for image segmentation and analysis. In this experiment, image-based method clearly can visualize and distinguish soft tissues including skin, tongue, muscles, brain, nerves and structures of the eye compare. This decomposition method is useful in clinical imaging and preclinical for vivo imaging of small animal models.
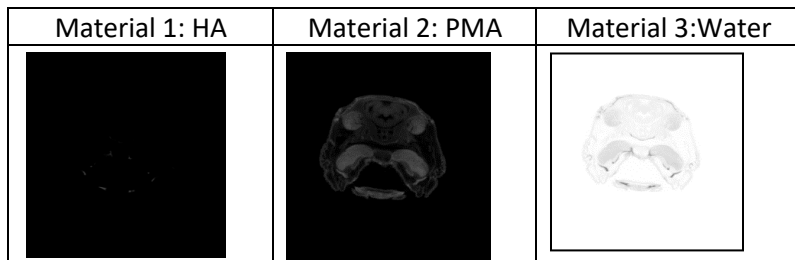
Material 1: HA	Material 2: PMA	Material 3:Water

Figure 2: The images result of decompose material by image-based method

4.2   Image decomposition for microchip sample
In this experiment, image-based method is used to get material-based image of material 1 and material 2 of microchip. In the data collection, the microCT scan transmission images of the object from multiple angular views when the object rotates on a high-precision stage. Based on Figure 3, the types of materials in the microchip on the image from two different energies which are 60 kVp and 100 kVp are not seen clearly. The effective linear attenuation coefficients (HU) values for each type of material in microchips must be determined as input parameter in image-based method. Therefore, the experiments have been conducted to obtain the ideal HU coefficients as input parameter in image-based method algorithm.

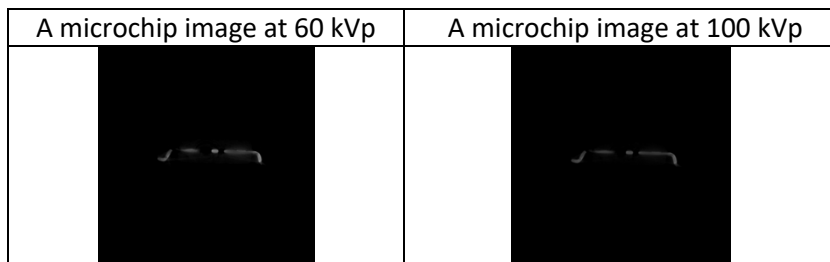| A microchip image at 60 kVp	A microchip image at 100 kVp

Figure 3: The images of microchip at 60 kVp and 100 kVp

By referring to the research work done by Ruder [8], the effective linear attenuation coefficients (HU) value of dual energy of different materials for DECT images are used as main reference. The range linear attenuation coefficient for each basic material for microchips have been obtained from experimental result and summarized in Table 3 to be used in the decomposition of the microchip images. Material 1 is defined as the outer layer of the microchip, Material 2 is the inner bar of the microchip while Material 3 is the "brightfield" image.

Table 3: Range of linear attenuation coefficient (HU) of basis material from experiment

Material	60 kVp	100 kVp
Material 1	2700-2900	1500-2000
Material 2	2000-2500	1000-1500
Material 3	0	0

In the data collection, the microCT scan transmission images of the object from multiple angular views when the object rotates on a high-precision stage. There are six sample of the images generated at different angles (260°, 262°, 264°, 266°, 268°, 270°) the microCT scanner.
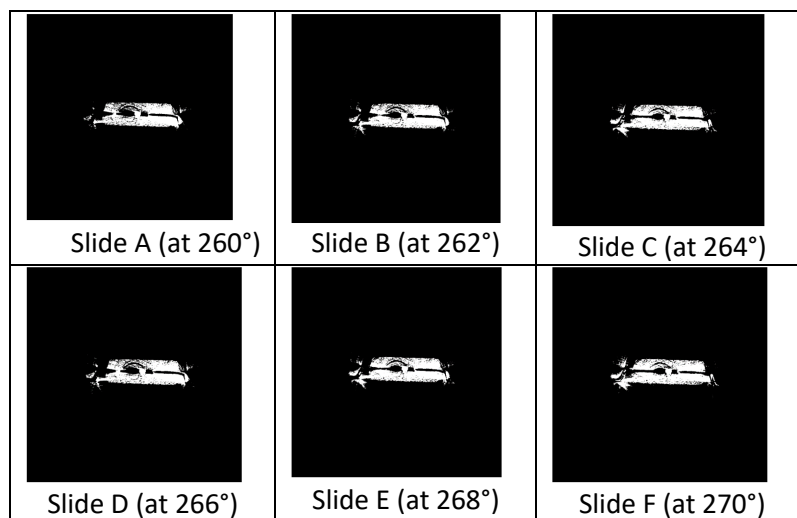

Slide A (at 260°)	Slide B (at 262°)	Slide C (at 264°)
Slide D (at 266°)	Slide E (at 268°)	Slide F (at 270°)

Figure 4: Material-specific image (Material 1)

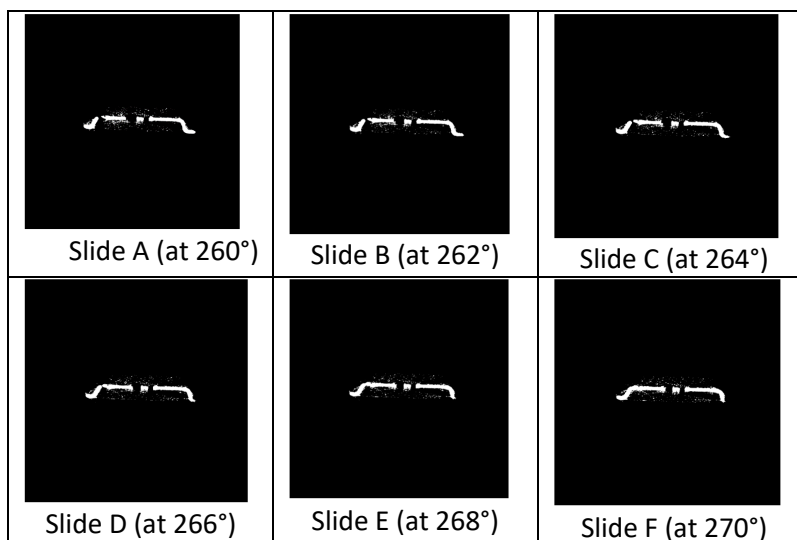|		
Slide A (at 260°)	Slide B (at 262°)	Slide C (at 264°)
Slide D (at 266°)	Slide E (at 268°)	Slide F (at 270°)

Figure 5: Material-specific image (Material 2)

Figure 4 shows the result of material-specific images for Material 1 of the six samples. From the observation, the outer layer of microchip is clearly seen with two layer: upper and lower layer for each sample. Besides, at the upper layer of the component, there is air gap, which means there are also other component at there might be a wire or some other materials. Figure 5 shows that material-specific image of Material 2 which is the inner bar of the microchip. There is a bar in the middle of the microchip has been clearly seen in the output images for each sample. From the observation of each sample images there are different size of air gap at the bar in each images. This is due to the input images are obtained from multiple angular views. Figure 6 shows the output of image decomposition for the brightfield images of the samples.
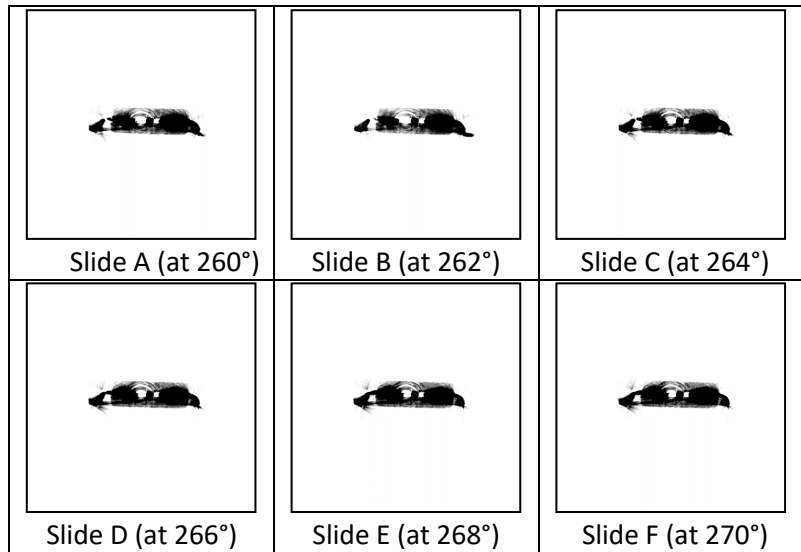

Figure 6: Material-specific image (brightfield)

From the observation through experimental results, material-specific results of each material for each sample with different angular view. Figure 7 show the original image and material-specific image of Slice A (at 260°).
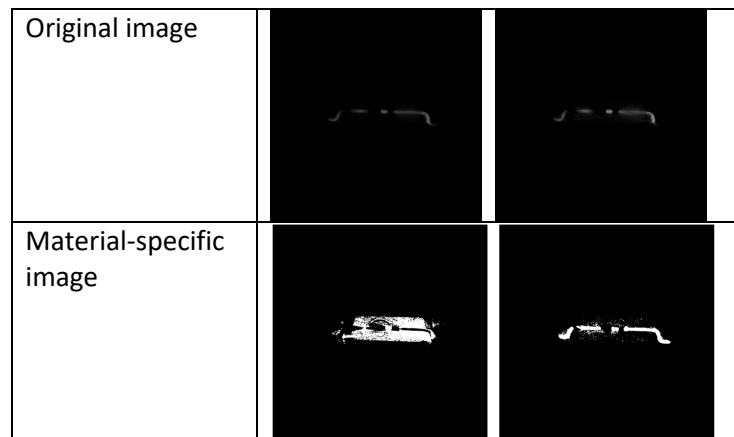

Figure 7: Comparison original image and material-specific image of Slice A (at 260°)

The purpose of considering multiple angular views dataset is to determine the angular view of microchip image that can be chosen as the best input image in this study. It is found that the material-specific images are different for each sample of material-specific image. Due to the microCT scan providing image of object with multiple angular view, an appropriate sample with specific angular view is important to be selected as input image in the further analysis. This is crucial to obtain reveal the exact shape of each microchip component in image decomposition with a correct input image. In the Figure 8(a), it is shown that the output image indicates an air gap (marked by red circle) between the bars of Sample A. Meanwhile, Figure 8(b) shows there is no air gap (marked by red circle) for the Material 2 of the microchip images. The main finding of this analysis is that choosing different sample produced from different angle views will give different results on material-specified images.

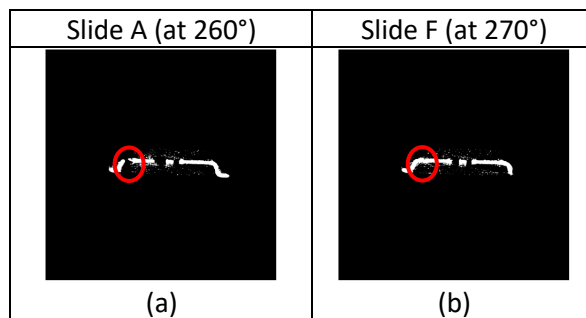| Slide A (at 260°)	Slide F (at 270°)
(a)	(b)

Figure 8: Comparison of the results of material-specified images at 260° and at 270°.

By comparing the computation decomposition results, taking appropriate input image with angle view of 270° is able to give the best output results compared to other angle views that tested in the experiments. Thus, to implement the image-based method in revealing the area of material of the microchips sample, the input images which generated by microCT scanner at angle 270° should be chosen.

4.3   Results validation

For the validation of the performance of image-based algorithm, the first experiment results had been done comparing the public available dataset that provided through research work published by Handschuh [6]. It was concluded that the vivo samples for decomposition between mineralized tissue and soft tissue. Further, the validation of the output image lies within the range of linear attenuation coefficient of basis material that obtained from this study through several experiments. Furthermore, the results of microchip image decomposition have been validated by an industry expert from Division of Industrial Technology in Malaysian Nuclear Agency, Kajang. It was certified that the material-specified images in this study show better visualisation results for each component (Material 1 and Material 2) compared to their original images. Based on her acknowledgment, this study with image-based method can be further developed and contribute into the computerized system that can automatically detected the improper or incomplete microchips though the DECT images captured by Micro-CT scanner. The experiments done on the microchips image for this study are expected to give better information in the future study for defective detection of microchips in semi-conduction industry.

5   Conclusion

In this study, image-based method was used to decompose the ex-vivo samples and microchips images to obtain material-specific images. These material-specific images can provide information of feature structure of tissues as well as materials of object through DECT images. The non-invasive technique is useful to analysis the condition of inner part of tissues or objects in decision making. For instance, the health condition of tissue can be monitored, and the quality of microchips can be assessed through the image decomposition. This study can be further continued the imaged based method can be then implementing in an automated computerized system to assist the engineers and inspectors to perform their task in inspections more efficiently. This computerized system is expected to replace the manual inspections, which is always time consuming when detecting the defective product.

References

[1]   Krasnicki, T., Podgorski, P., Guzinski, M., Czarnecka, A., Tupikowski, K., Garcarer, J., & Sasiader, M. (2012). Novel Clinical Applications of Dual Energy Computed Tomography. *Advance Clinical Exp. Medical 2012*, pp831-842.

[1]   Ryuta Mizutani, Akihisa Takeuchi, Kentari Uesugi, Susume Takekoshi, Yoshiyuki Osamura, & Yoshio Suzuki. (2008). X-ray Microtomographic Imaging of Three-Dimensional Structure of Soft Tissue. Tissue Engineering. doi:10.1089ten.tec.2008.0274.

[2]   Mouton, A., & Breckon, T. P. (2015). Material-based 3D segmentation of unknown objects from dual-energy computed tomography imagery in baggage security screening. doi: 10.1016/j.patcog.2015.01.010.

[3]   Siddiqui, S., & Khamees, A. A. (2004). Dual-energy CT-Scanning Application in Rock Characterization. SPE International.

[4]   Larsson, J. (2010). The use of Dual-Energy in Computed Tomography - a study of the first installed clinical CT using fast kV-switching at a children's hospital.

[5]   Handschuh S., Beisser C.J., Ruthensteiner B., & Metscher B.D. (2017). Microscopic dual-energy CT (microDECT): a flexible tool for multichannel ex vivo 3D imaging of biological specimens. Journal of Microscopy, pp3-26. doi:10.1111/jmi.12543.

[6]   Badea, C. T., Piantadosi, C. A., & Clark, D. (2016). Dual-energy micro-CT of the rodent lung. AJP Lung Cellular and Molecular Physiology. doi: 10.1152/ajplung.00359.2011.

[7]   Ruder, T., Bolliger, S. A., Thali, Y., & Thali, M. (2012). Material differentiation in forensic radiology with single-source dual-energy computed tomography. Forensic Science Medicine and Pathology. doi: 10.1007/s12024-012-9398-y.

[8]   Lev, M. H., & Gonzalez, R. G. (2002). CT Angiography and CT Perfusion Imaging, Brain Mapping: The methods (Second Edition), pp427-484. doi:10.1016/B978-012693019-1/50019-8.